BBAA VI International Colloquium on:
Bluff Bodies Aerodynamics & Applications
Milano, Italy, July, 20–24 2008

AERODYNAMIC INSTABILITY OF A BRIDGE DECK SECTION MODEL: LINEAR AND NONLINEAR APPROACH TO FORCE MODELING

G.Diana[†], D.Rocchi[†], T.Argentini[†] and S.Muggiasca[†]

Politecnico di Milano, via La Masa 1, 20156 Milano, Italy
Department of Mechanical Engineering
e-mails:giorgio.diana@polimi.it, daniele.rocchi@polimi.it,
tommaso.argentini@mecc.polimi.it, sara.muggiasca@polimi.it

Keywords: aerodynamic instability, bridge aeroelasticity, nonlinear effects, numerical simulation, hysteresis loop

Abstract: *The aerodynamic behavior of a bridge deck section model with a simple single-box shape was characterized in wind tunnel. At large nose-up mean angles of attack, a torsional instability arises, outlining a situation in which nonlinear aeroelastic effects may be critical. Such condition represents an interesting case to develop and validate nonlinear models for the aeroelastic problem. The experimental campaign allowed both to characterize the aerodynamic forces using forced motion tests and to study the aeroelastic behavior of the section model, when excited by actively generated turbulent wind. These aeroelastic tests are used to validate a numerical time-domain model for aerodynamic forces that takes into account the nonlinearities due to the reduced velocity and to the amplitude of the instantaneous angle of incidence. Results are critically analyzed and compared with those obtained with a linear model.*

Nomenclature

y	horizontal deck motion, positive along horizontal wind.
z	vertical deck motion, positive upward.
θ	torsional motion, positive if nose-up.
θ_m	mean angle of attack
V	average horizontal wind velocity component.
v	turbulent horizontal wind velocity component.
w	turbulent vertical wind velocity component.
ρ	air density.
B	deck chord length.
L	sectional model length.
ω	circular frequency of oscillation.
V^*_ω	reduced velocity $V^*_\omega = V/(\omega B)$.
V^*	reduced velocity $V^* = 2\pi V^*_\omega$.
ψ	instantaneous angle of attack, defined in eq.(4).
$\dot{\psi}$	time derivative of ψ.
a^*_j	j-th torsional flutter derivative.
χ_θ	torsional admittance function.
C_D	drag force coefficient; force is positive if along wind.
C_L	lift force coefficient; force is positive if upward.
C_M	pitching moment coefficient; moment is positive if nose-up.
β_j	coefficients of the model defined in eq.(5).
i	imaginary unit.

1 Introduction

The combination of large deck motion components and large turbulent components in wind velocity can induce large fluctuations of the instantaneous angle of attack. This is a critical aspect in aeroelastic analysis since large variations of the angle of attack may lead the deck to work in conditions in which nonlinear effects of aerodynamic forces are important. In such situations, linearized approaches (e.g. Jain et al. (1996); Minh et al. (1999); Chen et al. (2000); Caracoglia and Jones (2003)) show their intrinsic limits, whereas fully nonlinear approaches are required to model the deck response and they may provide a more accurate estimation of the instability onset. Nonlinear analyses (e.g. Diana et al. (1995); Minh et al. (1999); Chen and Kareem (2001); Zhang et al. (2002); Chen and Kareem (2003)) mainly focused on the nonlinear dependence of flutter derivatives and aerodynamic admittance functions on frequency. Recently Diana et al. (2008b) developed a promising model, based on the aerodynamic hysteresis loop concept, which accounts for nonlinear effects due to both frequency and amplitude of the instantaneous angle of attack.

In order to investigate the aerodynamic nonlinearities and their modeling, a wind tunnel experimental research was carried out on a deck section model (see Fig.1) at the Department of Mechanical Engineering of Politecnico di Milano. Experimental tests allowed a detailed aerodynamic characterization of a simple single-box shape deck that shows interesting nonlinear effects that lead to instability at large nose-up mean angles of attack. The wind tunnel tests allowed to define all the static and dynamic aerodynamic coefficients that are required by linear and nonlinear numerical modeling of the problem by means of forced motion tests (Diana et al., 2004). Furthermore, the experimental campaign allowed to measure the aeroelastic response

to turbulent wind when the deck section model is excited to vibrate under actively generated turbulent conditions with free motion tests (Diana et al., 2004). During these tests both forces and displacements of the elastically suspended model were contemporaneously recorded for different turbulent wind conditions. For this purpose the sectional model was equipped with a series of pressure taps to measure forces, while displacements were measured by an infrared measurement system during free motion tests and by laser transducers during forced motion tests.

A torsional instability at large nose-up mean angle of attack is present for a wide range of reduces velocities (neagative value of the $a*_2$ coefficient at $\theta_m = 6°$). Aeroelastic effects make the suspended sectional model prone to a 2-dofs instability, with an unusual torsional-lateral coupling. The control of the incoming turbulent wind allowed to investigate specific operating conditions where the deck is working close to instability and the small changes in the wind turbulence content may drive the deck behavior to cross the stability threshold.

These specific experimental tests, performed around a stable equilibrium configuration ($\theta_m \approx 3.5°$), highlight that a large amplitude of the instantaneous angle of attack, may lead the deck to work between stable and unstable conditions, which result in a dangerous limit cycle. This instability mechanism shows important nonlinear effects and therefore it represents an interesting case to develop and validate nonlinear numerical models for the aeroelastic problem. Therefore, such operating condition is used to validate the nonlinear numerical model (Diana et al., 2008b), whose results are compared with both experimental data and linear model results (Diana et al., 2005), in terms of forces and displacements.

In Section 2 we summarize the main characteristics of the experimental setup. The aerodynamic behavior using a linear approach is critically discussed in Section 3. In Section 4 nonlinear effects on instability are analyzed and modeled. The proposed nonlinear model is validated and compared with a linear one in Section 5. Final remarks are in Section 6.

2 Experimental setup

Wind tunnel tests were performed at Politecnico di Milano. Tests were designed to achieve the following goals: complete definition of aerodynamic and aeroelastic forces including effects of aerodynamic nonlinearities to compare linear and nonlinear approaches; complete aeroelastic characterization of the suspended section model, in terms of input (turbulent wind) and output (forces and displacements) for numerical model validations.

2.1 Deck section shape

Following the previous considerations, we studied a single-box deck section with a simple shape. The deck shape is taken from an actual highway bridge, but without the barriers on the upper surface. This simplification allows the measure of the aerodynamic forces directly through the integration of the pressure distribution. The deck section model is 2.91 meters long and the geometry and main dimensions of the section are reported in Fig.1.

2.2 Forcing systems

Three computer-controlled hydraulic actuators drive the forced motion tests, generating a multi-degree of freedom harmonic motion around a user-defined average angle of attack. Two different kinds of motion law were used to measure flutter derivatives and aerodynamic hysteresis loops: torsional motion and vertical motion.

In free motion test configuration, the model is suspended in the wind tunnel test section by

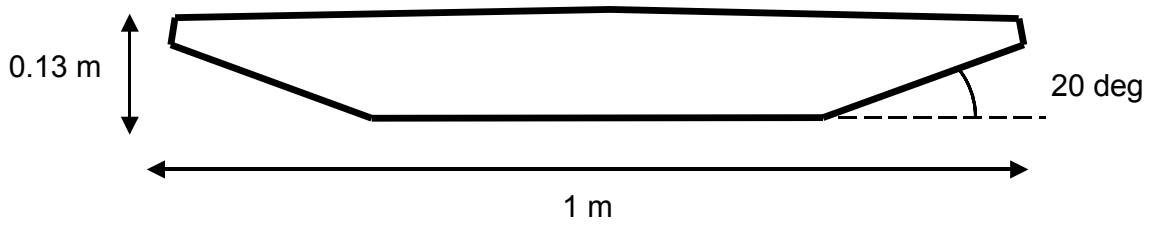

Figure 1: Deck section dimensions and shape

Figure 2: Experimental setup during forced motion tests

means of steel cables. A harmonic wind wave is generated by an active turbulence generator made by a horizontal array of 10 NACA 0012 profile airfoils, 4 m wide. The airfoils are driven by two brushless motors giving a pitching motion with a user-defined motion law in terms of frequency contents and amplitude. The turbulence generator is positioned 7 m upwind the model, while the incoming wind measure is performed one chord before the leading edge by means of a 4-holes probe that resolves the instantaneous vertical and horizontal wind components. A partial picture of the experimental setup is given in Fig.2.

2.3 Force measurements

A pressure measurement system was set up in order to prevent inertia forces subtraction problems during free motion tests (Diana et al., 2004). Pressure is measured on a ring of 78 pressure tabs around the middle section of the sectional model (see Fig.3), at a sampling frequency of 100 Hz. 16 pressure taps are distributes along four lines aligned with the deck axis , two in the upper part and two in the lower part, to measure the pressure distribution correlation in the axial direction. The distribution of the pressure taps was studied to refine the measure where strong pressure gradient are expected (see Fig.3). An example of pressure correlation along the deck axis is reported in Fig.4.

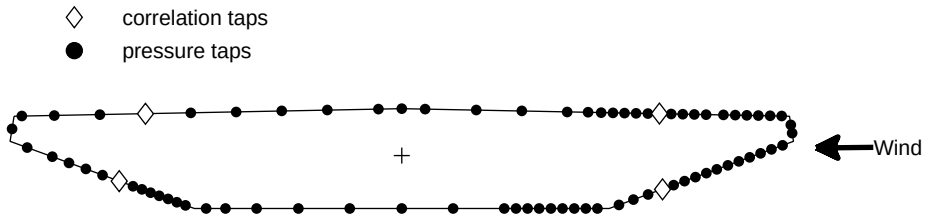

Figure 3: Pressure taps position

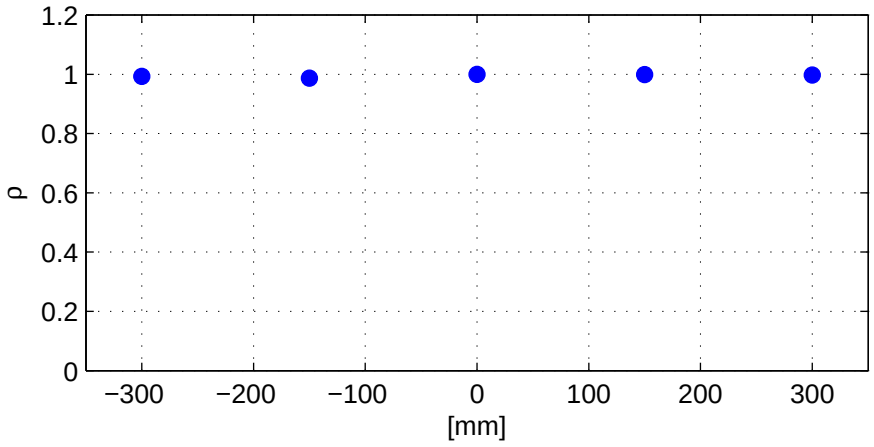

Figure 4: Pressure correlation along a correlation line

2.4 Motion measurements

During forced motion tests, two laser transducers measure the deck vertical and torsional displacement when the model is linked to the oil dynamic actuators. During free motion tests, a system of three infrared cameras allows a non intrusive measurement of the deck displacements. The model displacement is reconstructed by measuring the position of 10 markers located on the upper surface of the deck model. These markers reflect the infrared light that is emitted by specific stroboscopic lamps triggered with the camera sampling frequency (17 Hz). The marker position reconstruction is defined by the triangulation of the images recorded by a couple of cameras after a calibration procedure allowing for the correction of prospective and geometric aberrations Hartley and Zisserman (2003).

Pressure measurement were performed simultaneously with the camera measurements: since three different acquisition systems are used, with two different sampling frequencies, synchronization requires a particular care and a trigger signal was used for this purpose.

3 Characterization of aerodynamic forces and aeroelastic behavior

3.1 Linear analysis

The aerodynamic forces, i.e. drag (positive if windward), lift (positive if upward), and pitching moment (positive if nose-up), are usually separated into mean, self-excited and buffeting force components. The mean averaged (static) forces per unit length are expressed as

$$L_s = \frac{1}{2}\rho V^2 B C_L(\theta_m); \quad D_s = \frac{1}{2}\rho V^2 B C_D(\theta_m); \quad M_s = \frac{1}{2}\rho V^2 B^2 C_M(\theta_m), \tag{1}$$

where ρ is the air density; V is the mean wind horizontal velocity; B is the deck chord; C_D, C_L and C_M are the mean lift, drag and pitching moment coefficients; θ_m is the mean angle of the section.

Self-excited forces resulting from structural motion can be expressed in terms of flutter derivatives, which are function of the oscillation frequency . According to the formulation proposed by Zasso (1996), the pitching moment per unit length is:

$$M_{se} = \frac{1}{2}\rho V^2 B^2 \left(-a_1^* \cdot \frac{i\omega z}{V} - a_2^* \cdot \frac{i\omega \theta B}{V} + a_3^* \cdot \theta + a_4^* \cdot \frac{\pi}{2V_\omega^{*2}} \cdot \frac{z}{B} \right.$$
$$\left. - a_5^* \cdot \frac{i\omega y}{V} + a_6^* \cdot \frac{\pi}{2V_\omega^{*2}} \cdot \frac{y}{B} \right), \tag{2}$$

where a_j^* ($j = 1 \ldots 6$) are the torsional flutter derivatives; y, z and θ are the horizontal, vertical and torsional displacements; ω is the circular frequency of oscillation; i is the imaginary unit; $V_\omega^* = V/(\omega B)$ is the reduced velocity. Analogous formulations hold for lift and drag forces, in order to define the complete set of 18 flutter derivatives (Zasso, 1996).

Buffeting forces, resulting from turbulent wind components, can be expressed in terms of aerodynamic admittance functions, which are function of the wind oscillation frequency. In this case, the pitching moment per unit length is given by:

$$M_b = \frac{1}{2}\rho V^2 B^2 \left(\chi_{\theta w} \frac{w}{V} \right), \tag{3}$$

where $\chi_{\theta w}$ is the complex torsional admittance function; w is the vertical turbulent wind velocity fluctuation. Analogous formulations hold for lift and drag forces (Diana et al., 2005).

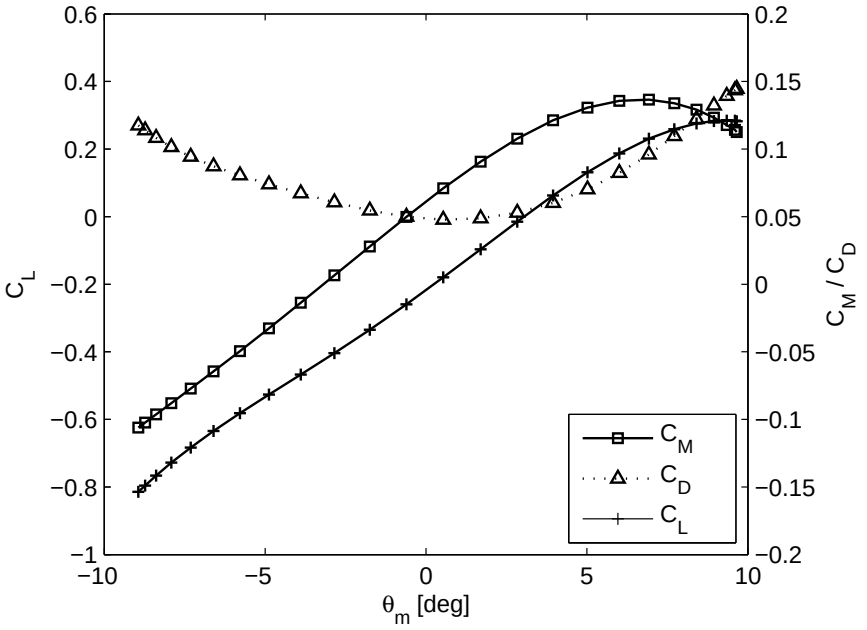

Figure 5: Static coefficients at different θ_m

For the examined cross section, the static aerodynamic force coefficients as a function of the angle of attack are shown in Fig.5. We can remark the following characteristics: drag coefficient has a minimum at $\theta_m = 1°$; lift coefficient has a positive slope $\left(\frac{\partial C_L}{\partial \theta} > 0\right)$ up to $\theta_m = 9°$ where it has a maximum (stall) followed by a negative slope; moment coefficient is positive at $\theta_m = 0°$ and it has a positive slope up to $\theta_m = 6°$, where it stalls; moment stall occurs before lift stall. These characteristics may lead to a torsional instability in quasi-steady conditions.

If we explore the force dependence upon the frequency of excitation and we analyze the self-excited forces, focusing on the effects of torsional displacement θ, according to equation (2), a negative value of the a_2^* coefficient results in a direct negative damping term, which reduces stability margins.

Flutter derivatives a_2^* and a_3^*, shown in Fig.6, highlight that torsional instability for large angles of attack is present in at large reduced velocities ($a_2^* \rightarrow \frac{\partial C_M}{\partial \theta}\big|_{\theta_m}$ for $V^* \rightarrow \infty$), and it decreases with decreasing reduced velocity, up to disappearing at $V^* = 6$ for $\theta_m = 6°$.

Analogous considerations can be done for buffeting forces. Considering the $\chi_{\theta w}$ function and interpreting $\frac{w}{V}$ as an instantaneous angle of attack, it is clear that its effect is analogous to an instantaneous angle of attack $\frac{\dot{z}}{V}$. This fact is confirmed by comparing the trend of the a_1^* coefficient with the one of the real part of $\chi_{\theta w}$, as shown in Fig.7. The linear aerodynamic behavior is clearly identified by θ_m and by the slopes of static coefficients around the value of θ_m.

3.2 Nonlinear effect of instability threshold

Torsional instability is experienced not only when the mean angle is sufficiently large to have a negative a_2^*, but also when the instantaneous angle of attack, due to both deck motion and turbulent wind, reaches large oscillation amplitudes around a static value within the stability range. This phenomenon is clearly pointed out by wind tunnel tests performed on the deck section model elastically suspended and run over by an actively generated turbulent wind.

The structural characteristics of the oscillating section model in no-wind conditions are re-

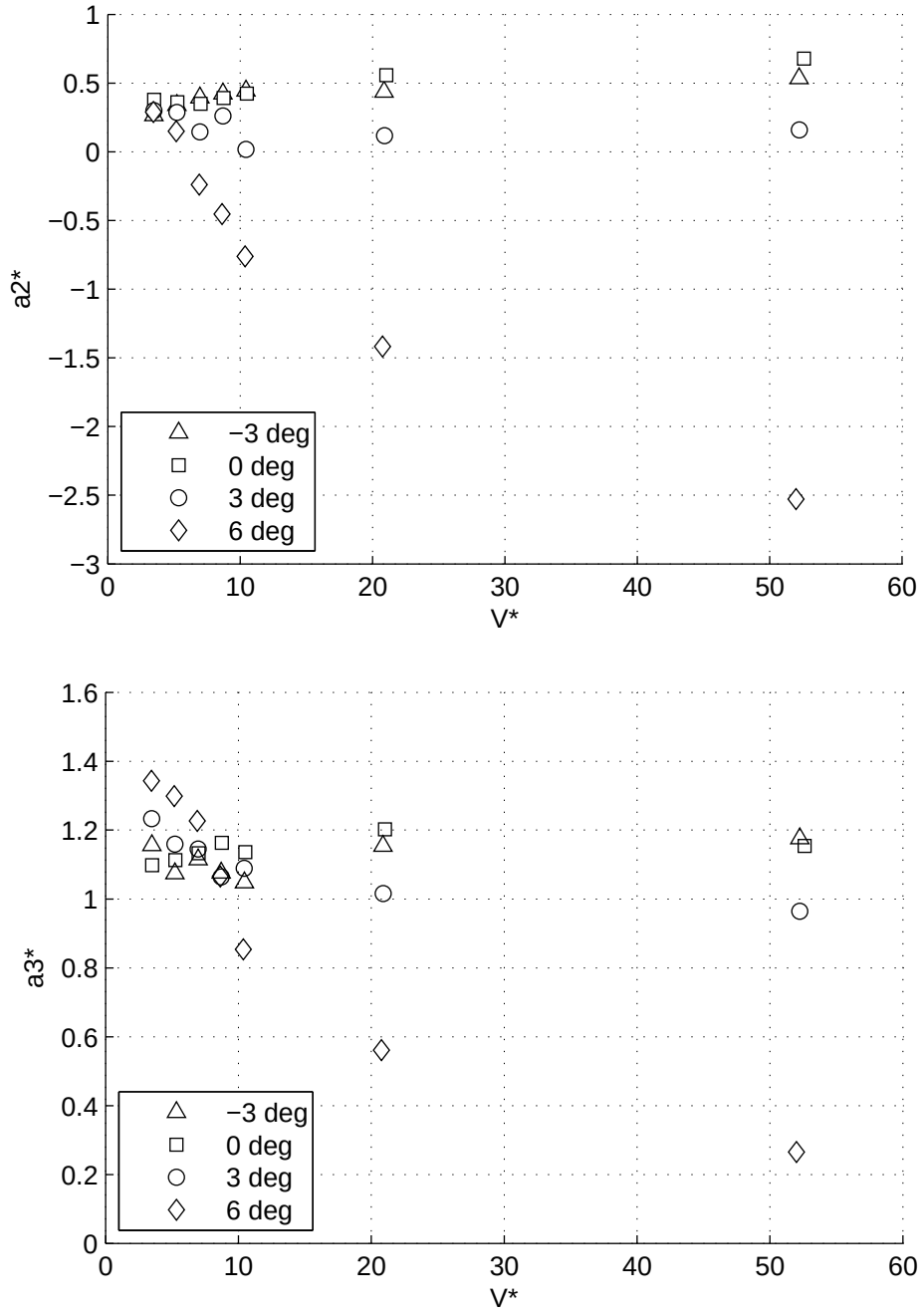

Figure 6: Torsional flutter derivatives at different θ_m vs. V^*

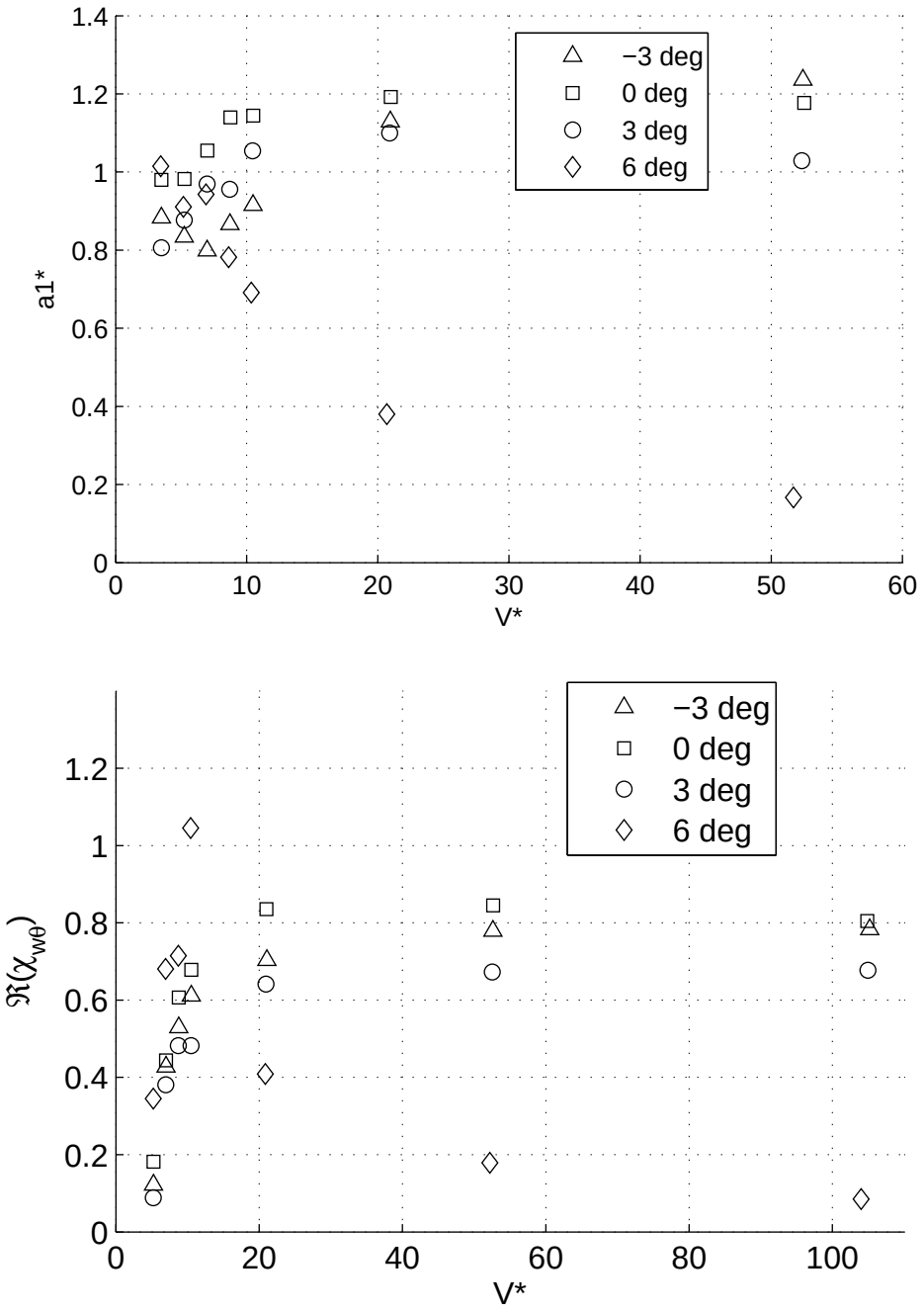

Figure 7: Torsional flutter derivative a_1^* and real part of $\chi_{\theta w}$ at different θ_m vs. V^*

Mode	Type	Frequency	Mass	Damping %
1	Horizontal	$0.74\ Hz$	$68\ Kg$	0.23
2	Torsional	$0.99\ Hz$	$8.3\ Kgm^2$	0.30
3	Vertical	$1.09\ Hz$	$68\ Kg$	0.94

$$\begin{bmatrix} y \\ z \\ \theta \end{bmatrix}_1 = \begin{bmatrix} 1 \\ -0.15 \\ 0.38 \end{bmatrix}, \qquad \begin{bmatrix} y \\ z \\ \theta \end{bmatrix}_2 = \begin{bmatrix} 0.025 \\ 0.005 \\ 1 \end{bmatrix}, \qquad \begin{bmatrix} y \\ z \\ \theta \end{bmatrix}_3 = \begin{bmatrix} 0 \\ 1 \\ 0.15 \end{bmatrix}$$

Table 1: Modal properties and eigenshapes of suspended section model

ported in Tab.1. These values were obtained analyzing the decay of free motion tests experienced by the aeroelastic model starting from imposed initial motion condition in still air. Similar analysis performed under mean wind flow conditions highlighted the aeroelastic effects on the values of mean angle θ_m, frequencies and torsional damping. These effects are reported as a function of the mean velocity V in Fig.8. An increasing wind speed has a twofold effect: on one side, an increase of the mean angle of equilibrium due to the positive value of the moment coefficient (nose-up); on the other side, there is a softening in the torsional frequency, which collapses toward the horizontal one, giving rise to a 2-dofs instability close to $V = 8\ m/s$, where the total damping (structural plus aerodynamic) becomes negative.

Considering a mean wind velocity of $7\ m/s$, the model assumes a mean angle $\theta_m = 3.5°$ that, according to a linear approach and previous results, guarantees a stable behavior for any turbulent wind condition. In fact, by superimposing a harmonic turbulent wind component, such to get an instantaneous wind angle $\frac{w}{V} = 0.5°$, with frequency of $0.7\ Hz$ and reduced velocity $V^* = 10$, the model oscillates with small amplitudes around the static angle of attack, as shown in Fig.9(a). However, with a doubled wind angle $\frac{w}{V} = 1°$, the response is about ten times greater, as shown in Fig.9(b).

In the latter case, the amplitude of the variation of the instantaneous angle of attack is large enough to drive the deck model in and out of the instability range, resulting in very large torsional oscillations. This behavior is strongly nonlinear and it cannot be foreseen by a linear approach.

4 Nonlinear analytical formulation

4.1 Aerodyanamic hysteresis loops

A founding hypothesis of the linear approach is that only small perturbations of the angle of attack occur around a static configuration. However, to simulate the experimental instability onset, we pointed out the necessity of considering the effects induced by a large variation of the angle of attack.

An interesting nonlinear analytical representation of the aerodynamic forces by means of hysteresis loops has been proposed by Diana et al. (2007, 2008a,b). In Fig.10, we show the effect of the angle of attack amplitude on the pitching moment at $V^* = 10$, obtained with harmonic forced torsional motion tests, by drawing the aerodynamic moment coefficient versus the angle of rotation θ. The area enclosed by the loops represents the work done by the aerodynamic moment in one oscillation cycle and it is an index to assess whether energy is dissipated or pumped into the system. The direction of rotation of the loop indicates the relative phase between force and displacement and therefore the energy sign: clockwise (+ circles)

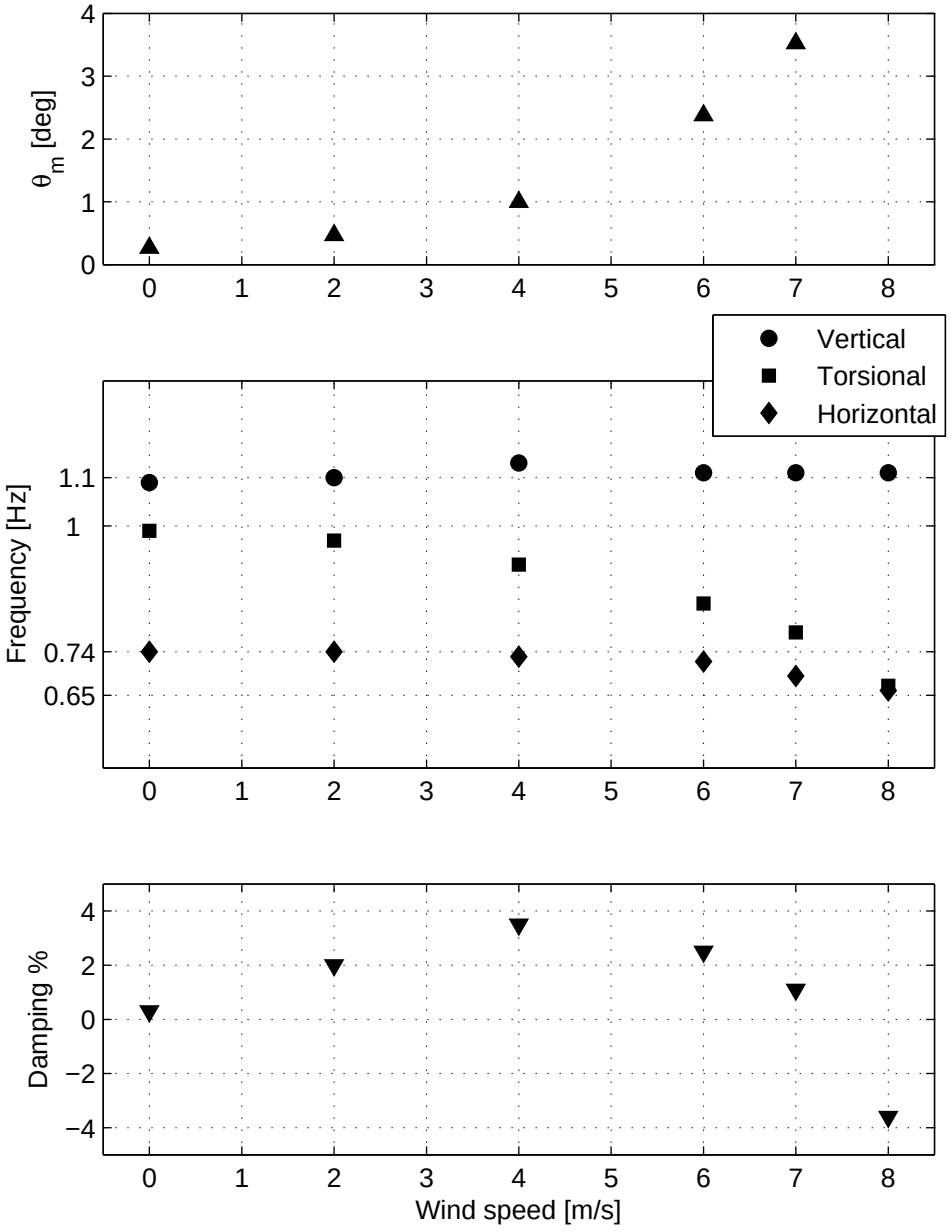

Figure 8: Aeorelastic effects of mean wind velocity: mean angle θ_m, natural frequencies and torsional damping

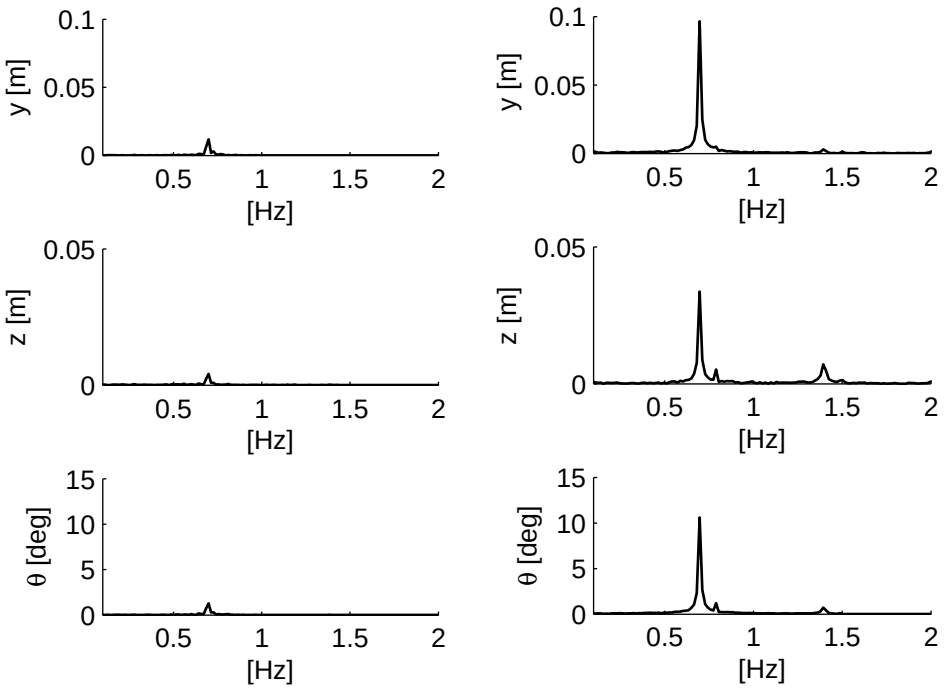

(a) $\frac{w}{V} = 0.5°$ at $0.7\ Hz$ (b) $\frac{w}{V} = 1°$ at $0.7\ Hz$

Figure 9: Frequency response of the aeroelastic model under two different turbulent wind conditions

indicates energy pumping, anticlockwise (- circles) indicates energy dissipation. Such representations permit a phenomenological interpretation of the torsional instability: loops with small amplitudes of oscillation (up to $2.5°$) dissipate energy (upper plots of Fig.10); increasing the amplitude, the hysteresis loop twists generating an energy pumping contribution beside the dissipation one. This contribution increases with larger amplitudes and, for sufficiently large oscillations, it cancels out the dissipative part of the loop, pumping energy into the system during almost all the cycle.

The nonlinear model (Diana et al., 2008a) lies on the hypothesis that aerodynamic aeroelastic and buffeting forces are function of the instantaneous angle of attack ψ, defined as:

$$\psi = \theta + \tan^{-1}\left(\frac{b^*\dot{\theta} - \dot{z} + w}{V + v - \dot{y}}\right), \tag{4}$$

where b^* is a constant length, assumed to be $B/2$. Once defined ψ, hysteresis loops can be represented as functions of it.

The above assumption implies that, for a given instantaneous angle of attack, forces are defined independently on whether ψ is generated by either deck motion or turbulent wind or by a combination of the two. In Fig.11, we compare hysteresis loops resulting from two differently generated variations of ψ, with equal amplitudes and reduced velocity: results from imposed torsional motion tests are shown in Fig.11(a), while those from imposed turbulent vertical wind component are shown in Fig.11(b). Loops at the same V^* show good agreement supporting the hypothesis; a remark about the $V^* = 8$ is that the loop due to turbulent wind has a smaller amplitude due to the physical limits of the active turbulence generator which does not allow for

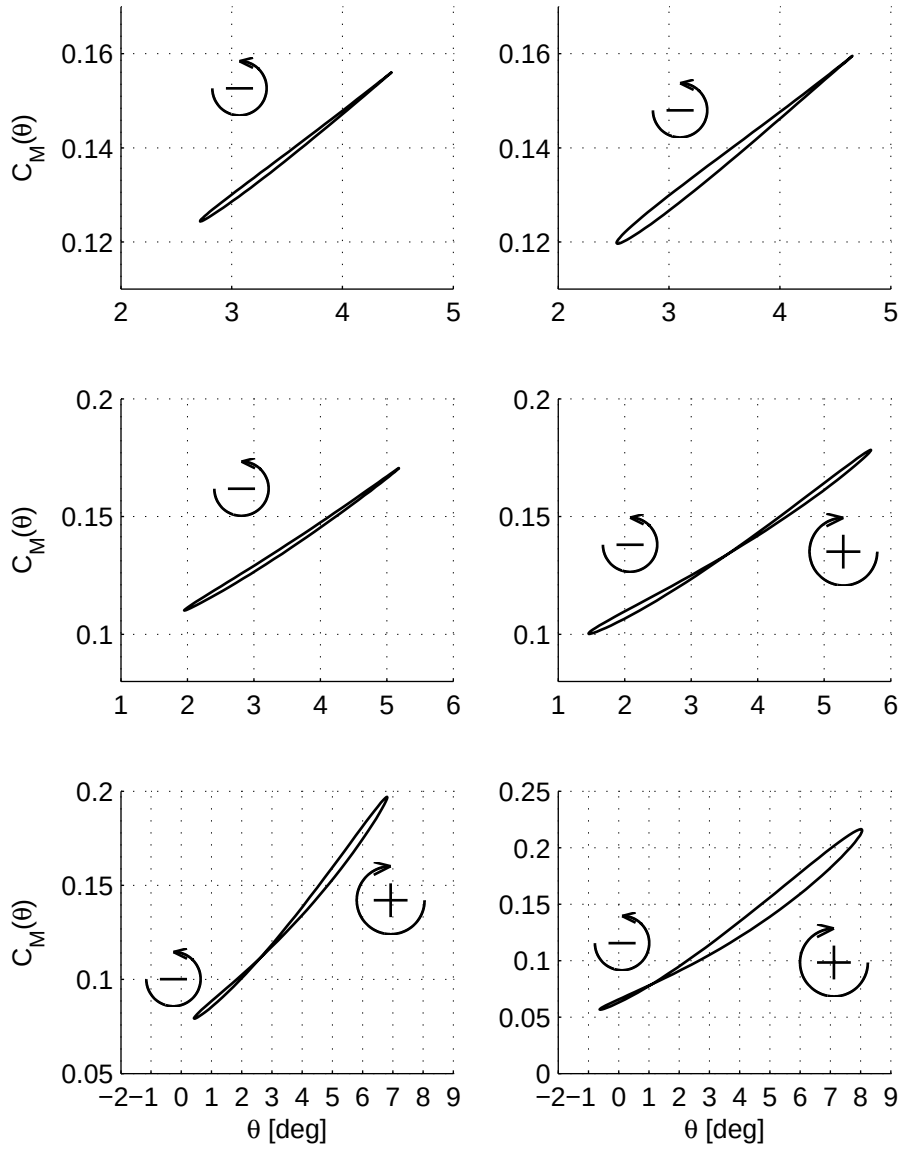

Figure 10: Hysteresis loops of moment coefficient considering different amplitudes of the angle of attack at $V^* = 10$, $\theta_m = 4^\circ$

large amplitudes of the angle of attack at high frequencies.

The dependency on the amplitude of torsional oscillation, for the moment coefficient, is shown in Fig.12 for the same θ_m and V^*: using ψ instead of θ, the complex shapes of Fig.10 become more regular and the loops rotate in the same direction, resulting in an easier way to identify the parameters of the numerical model that will be presented in the next paragraphs. Analogous considerations hold for the drag and lift coefficients.

4.2 Nonlinear time-domain model of aerodynamic hysteresis loops

This nonlinear framework is suitable for formulating nonlinear models (Diana et al., 2007, 2008a,b). The proposed nonlinear time-domain model is a nonlinear polynomial function of the dynamic angle of attack ψ and of its time derivative whose parameters are identified using the experimental data obtained at different reduced velocities with the torsional forced harmonic motion tests at large oscillation amplitude. The expression for moment coefficient is:

$$\begin{aligned} C_M(\psi,\dot{\psi}) = C_M^{static}(\psi) + \ldots \\ \beta_1 + \ldots \\ \beta_2\psi + \beta_3\dot{\psi} + \ldots \\ \beta_4\psi^2 + \beta_5\psi\dot{\psi} + \ldots \\ \beta_6\psi^3 + \beta_7\psi^2\dot{\psi}, \end{aligned} \tag{5}$$

where β_j $(j = 1 \ldots 7)$ are constant parameters and C_M^{static} is the static coefficient. β_i coefficients are identified using a weighted least square curve fitting algorithm that minimizes the error between the experimental hysteresis loops and the ones produced by the numerical model using a wide range of reduced velocities ($V^* = 7 \div 200$). During the identification procedure, higher weight was assumed for lower operational reduced velocities.

Such a model, however, is not able to reproduce the nonlinear effect of the instability threshold presented in paragraph 3.2. The dependency of instability on the amplitude of the angle of attack ψ needs a model that has a rheologic element able to simulate the strong nonlinear effect of amplitude on stability. This can be achieved introducing the rheologic element schematically depicted in Fig.13. In this scheme, the modeled moment coefficient is equal to the force transmitted to the ground by the equivalent mechanical system sketched in Fig.13. The rheologic element is activated only if the following conditions are met:

1. $\psi > \psi_{\text{threshold}}$ when $\dot{\psi}$ becomes negative
2. $\dot{\psi} < 0$

Condition 1 is an on-off switch that activates a viscous element with negative damping, which remains active till condition 2 is valid. This asymmetric behavior is clearly evidenced by the shape of pitching moment hysteresis loops in Fig.12.

5 Model validation

5.1 Validation in the stability range

Since the proposed approach is aimed to define a methodology to foresee the aeroelastic behavior of bridges in real operating conditions, the model is validated around a stationary configuration of $\theta_m \approx 0°$. To achieve this configuration, and to maintain simultaneously a

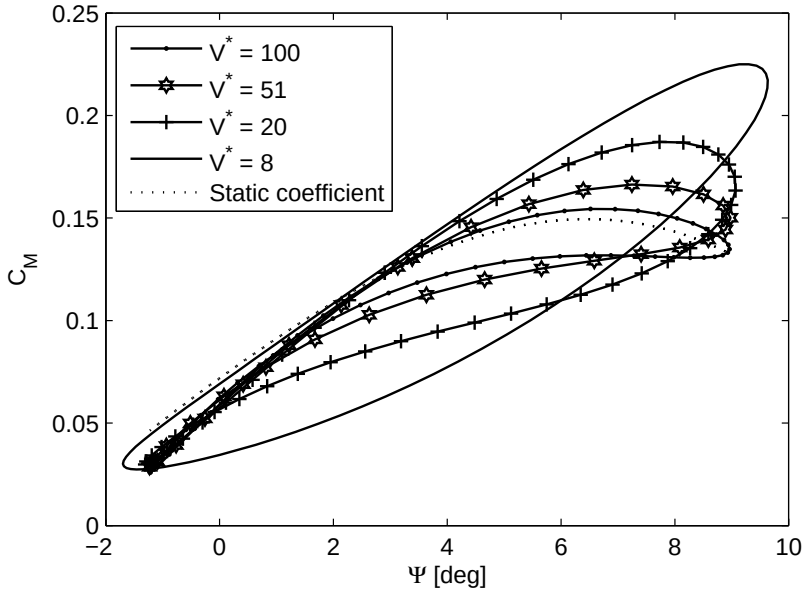

(a) ψ due to forced torsional motion

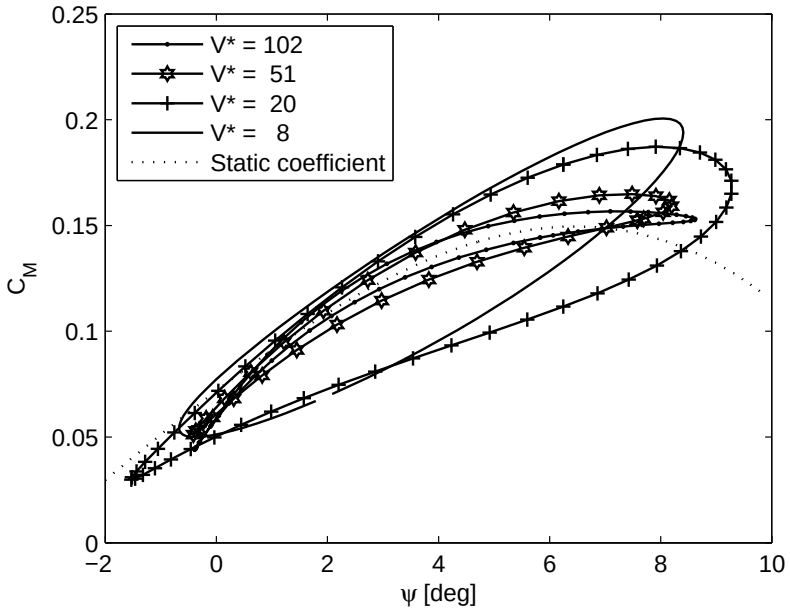

(b) ψ due to turbulent wind

Figure 11: Moment coefficient vs. ψ, at different V^*

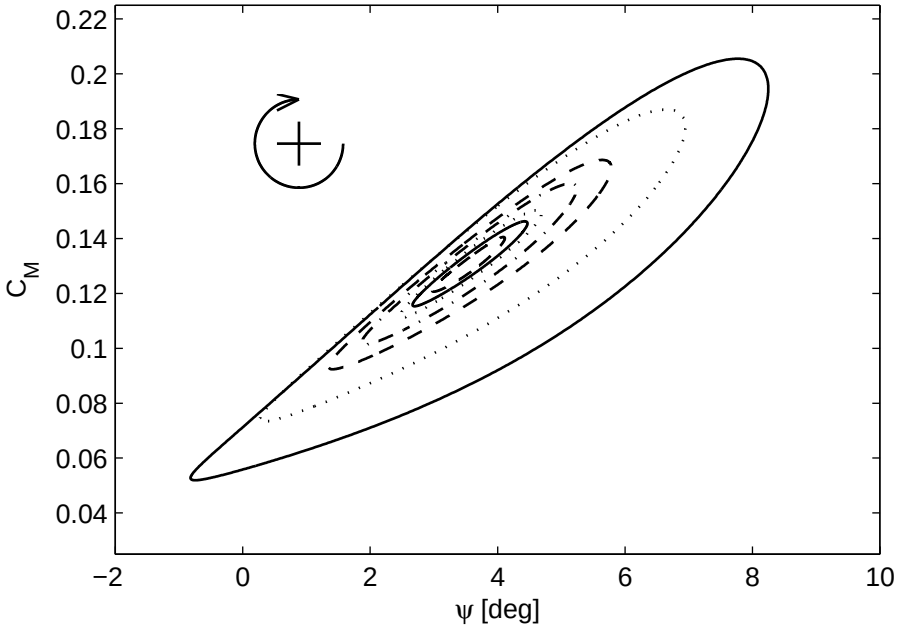

Figure 12: Moment coefficient vs. ψ, with varying amplitudes of the instantaneous angle of attack, at $V^* = 10$

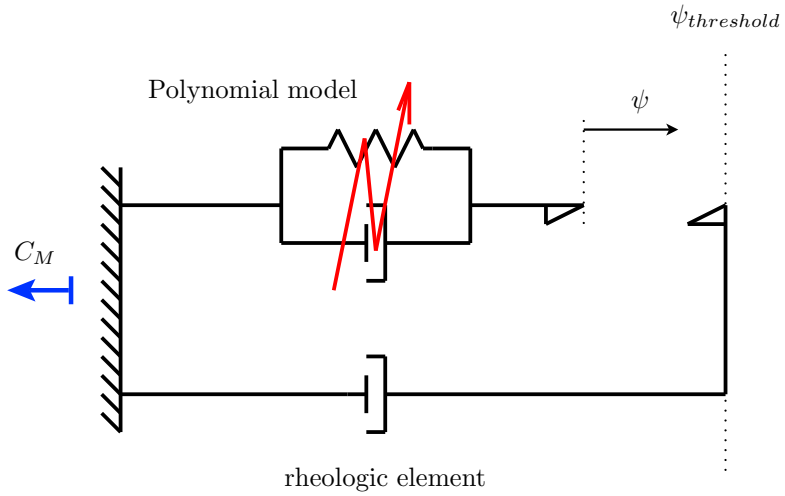

Figure 13: Rheologic scheme for nonlinear instability

sufficiently large wind velocity ($8\ m/s$), the no-wind starting configuration was properly set with a negative pitch, letting the positive aerodynamic moment to bring the model at $\theta_m \approx 0°$.

In Fig.14 we present the results of the identification procedure for all the three aerodynamic coefficients at several V^*, obtained using forced torsional motion tests.

The model is then validated against aeroelastic free motion tests, comparing aerodynamic forces and displacements. In addition, results obtained with a linear approach using flutter derivatives and admittance functions are compared to stress the need for nonlinear modeling. Two different test cases are considered: in case A the suspended model is forced by a mono-harmonic turbulent vertical wind component w with amplitude $\frac{w}{V} = 3°$ at a frequency of $0.37\ Hz$; in case B the suspended model is forced by a mono-harmonic turbulent wind w with amplitude $\frac{w}{V} = 3.8°$ at a frequency of $0.57\ Hz$. Experimental measurements of the vertical turbulent wind components for both cases are reported in Fig.15. The horizontal wind component is in both cases equal to $8\ m/s$.

Case A is an interesting test-case because the second order harmonics of the aerodynamic forces excite the horizontal mode, while third order harmonics excite the third mode. Experimental and numerical comparisons are shown in Figs.16 and 17.

In case B a large dynamic angle of attack is created by the combination of wind and deck motion, and the second harmonic generated by nonlinearity of drag excites the vertical mode. Experimental and numerical comparisons are shown in Figs.18 and 19.

As a general comment, in both test-cases numerical simulations show how the linear approach based on the flutter derivatives and admittance function formulation is not able to predict the actual response with second and third order harmonics. Focusing on the first harmonic, drag force is underestimated, since the aerodynamic coefficients are considered at the static mean angle of attack and, in the case of drag, the curve has an almost null slope. The presence of a second harmonic in the drag force is due to the projection of the first harmonic of the lift along the local reference system. On the contrary, the nonlinear approach is able to reproduce the nonlinear effects, generated by large dynamic angles of attack, which strongly interact with structural coupling.

5.2 Validation in the instability range

In order to show the need for the rheologic element, in Fig.20 we present the results of the identification procedure for the aerodynamic moment coefficients at several amplitudes of the angle of attack around a static value of $\theta_m = 3.5°$.

Hysteresis loops in Fig.20(a) are obtained using the polynomial model and excluding the rheologic element, while loops in Fig.20(b) are obtained including it and they can bre compared with the experimental values of Fig.12. It is evident that the polynomial model alone cannot reproduce the asymmetry of the aerodynamic coefficients, which is responsible for the amplitude driven instability, as already discussed in paragraph 4.1. On the contrary, the introduction of the rheologic element allows to include and simulate effectively this effect.

The amplitude driven rheologic element in combination with the polynomial terms allows to reproduce the nonlinear aeroelastic behavior described in paragraph 3.2 as well. Numerical results presented in Fig.21 show how the nonlinear dependence on the amplitude of the angle of attack ψ is reproduced. In Fig.21(a) it is shown the deck torsional motion with a vertical turbulent wind excitation angle of $0.5°$, whereas in Fig.21(b) it is reported the torsional motion due to a wind angle with double amplitude, which clearly points out the nonlinear behavior of the deck.

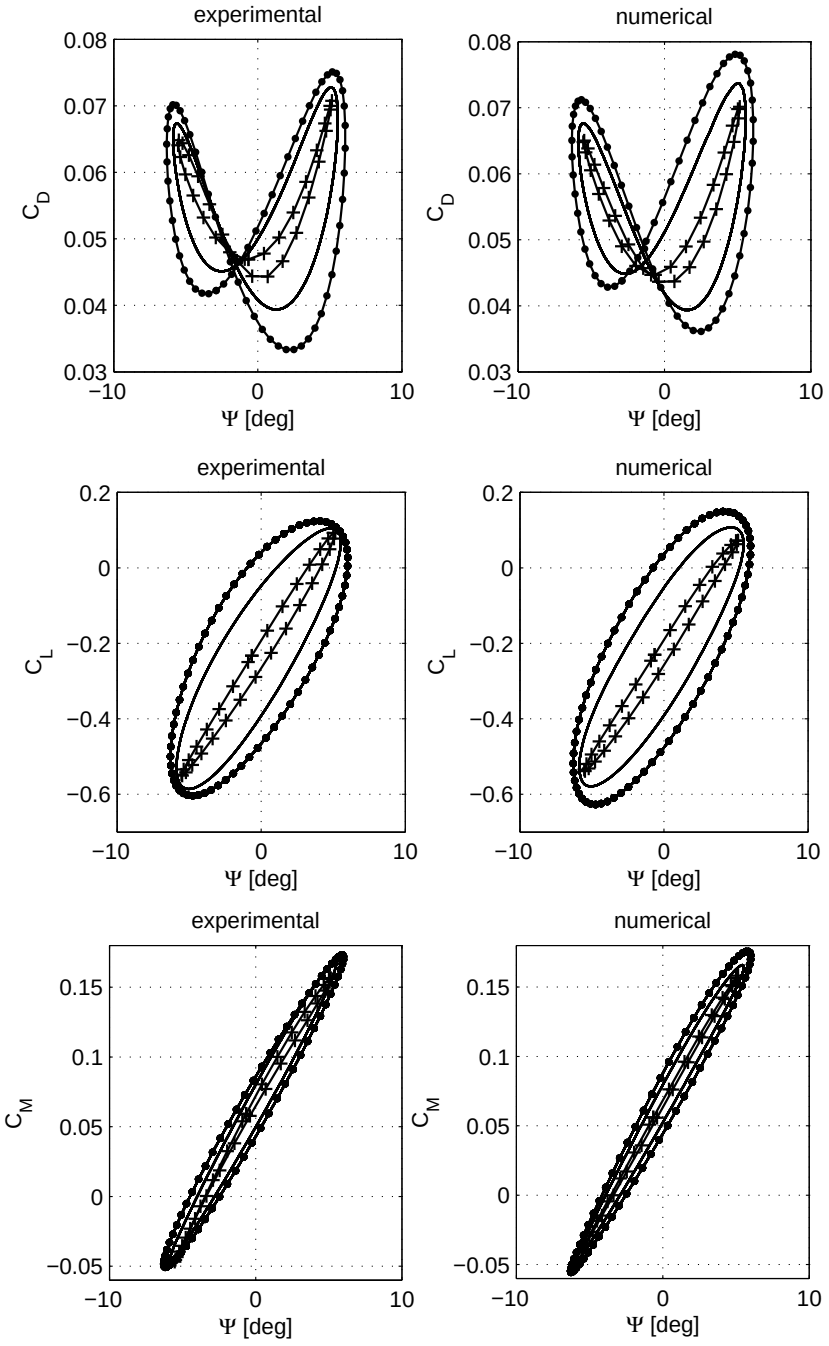

Figure 14: Numerical hysteresis loops compared with the experimental ones at $V^* = 7$ (pointed line), $V^* = 10$ (solid line), $V^* = 50$ (diamonds)

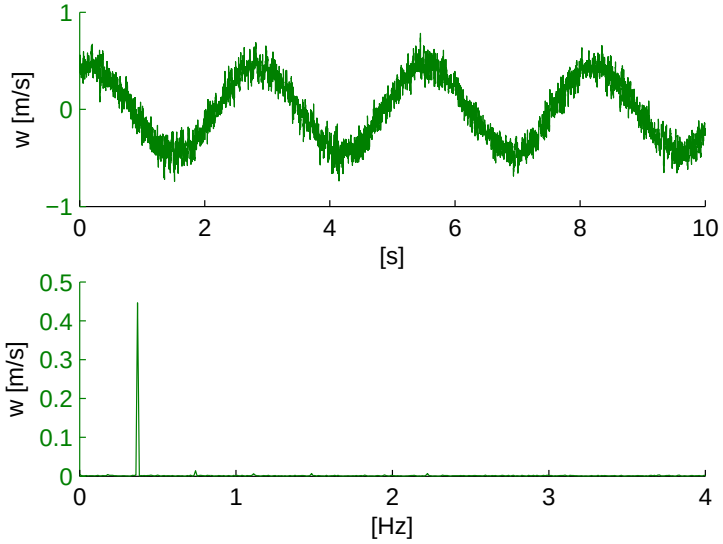

(a) case A

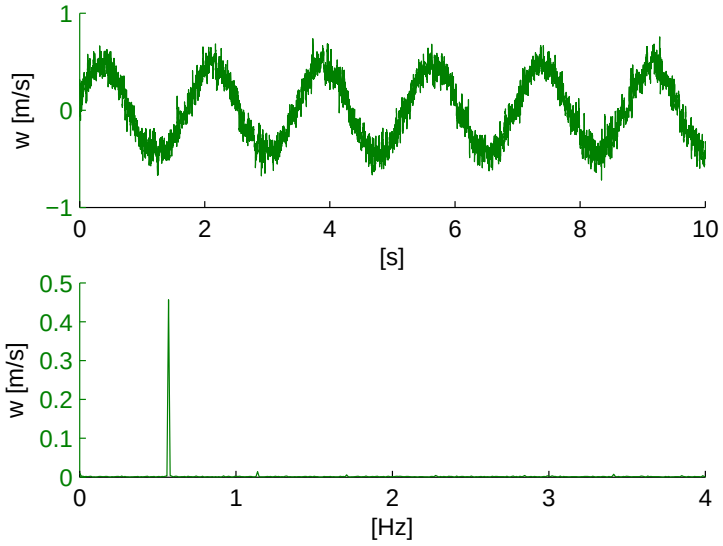

(b) case B

Figure 15: Experimental turbulent vertical wind components for case A and B. In both cases the horizontal component is equal to $8\ m/s$

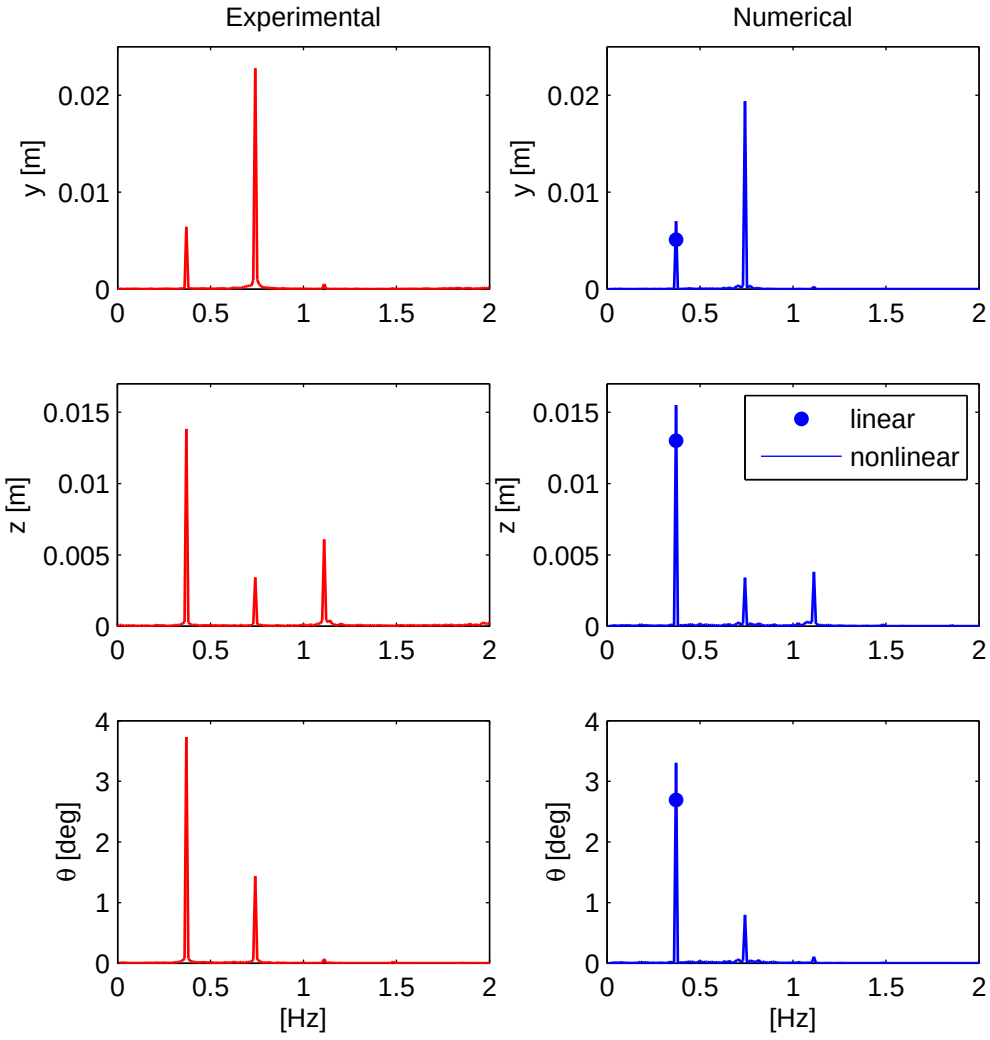

Figure 16: Case A: global displacements

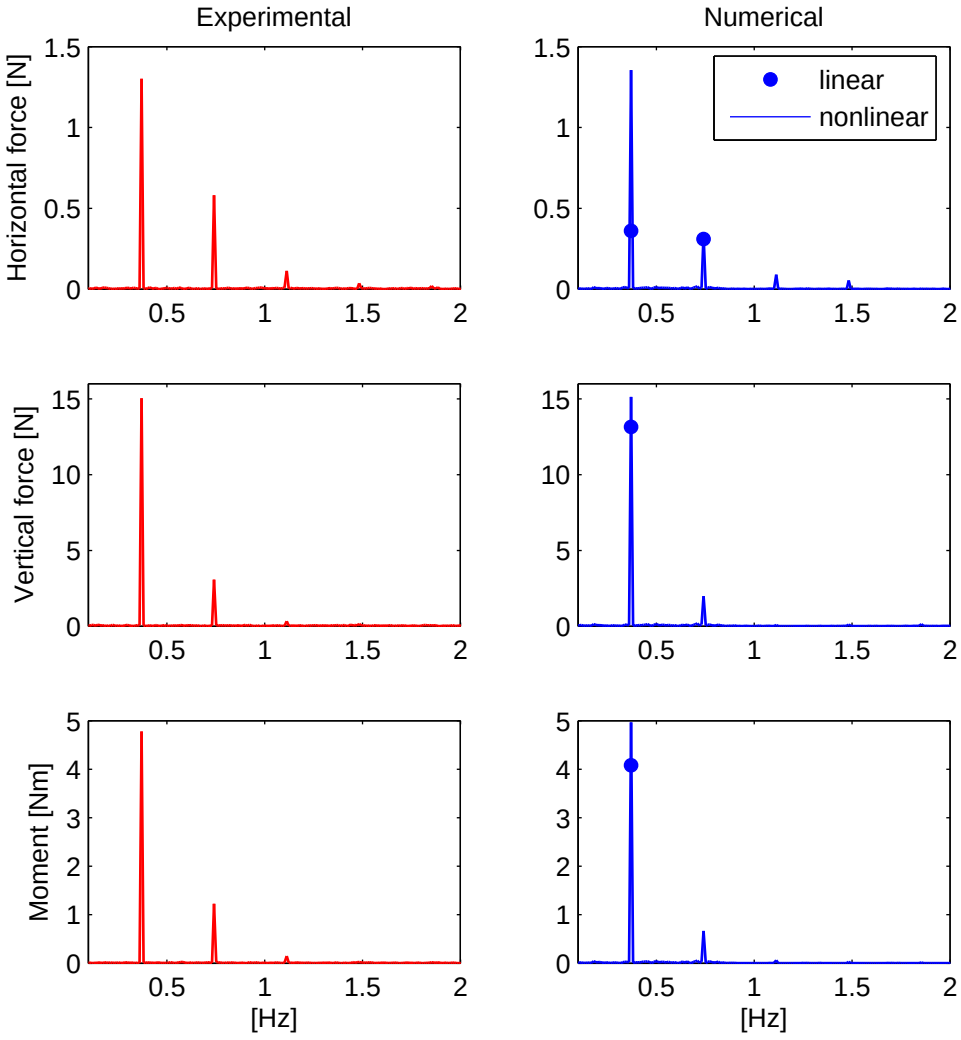

Figure 17: Case A: forces in a reference system fixed to the deck

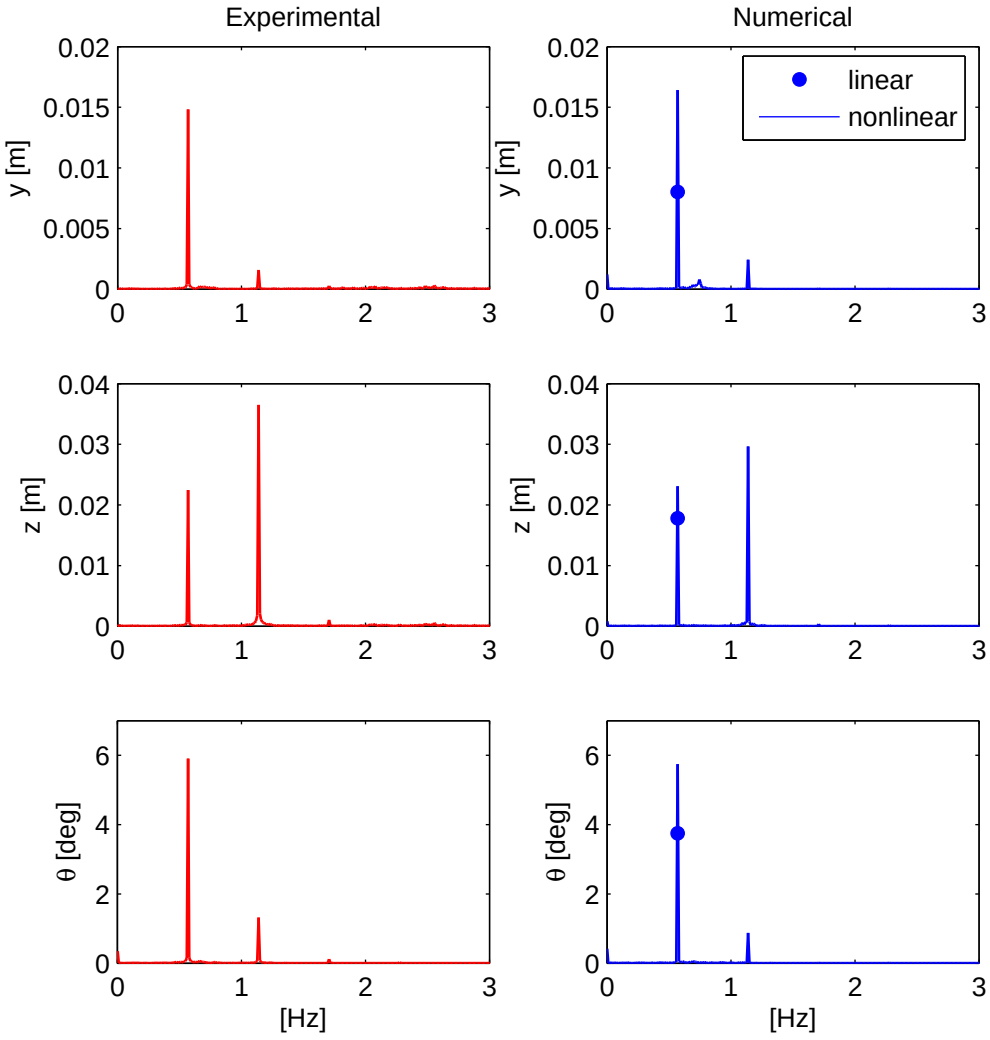

Figure 18: Case B: global displacements

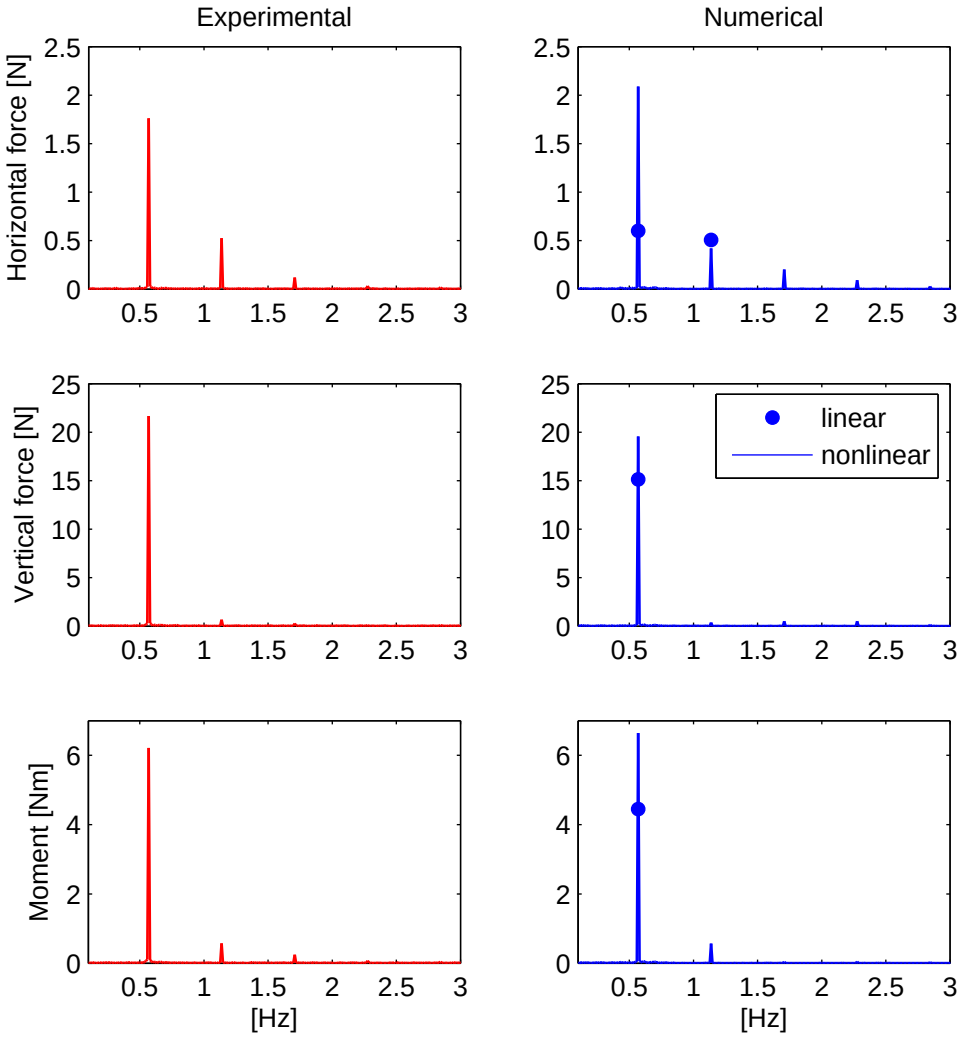

Figure 19: Case B: forces in a reference system fixed to the deck

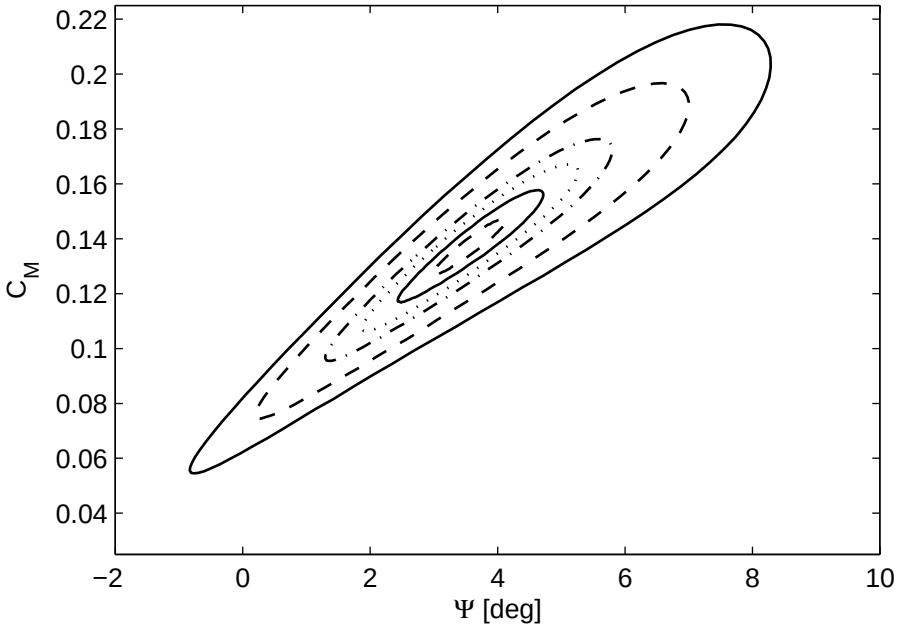

(a) Loops without the rheologic element

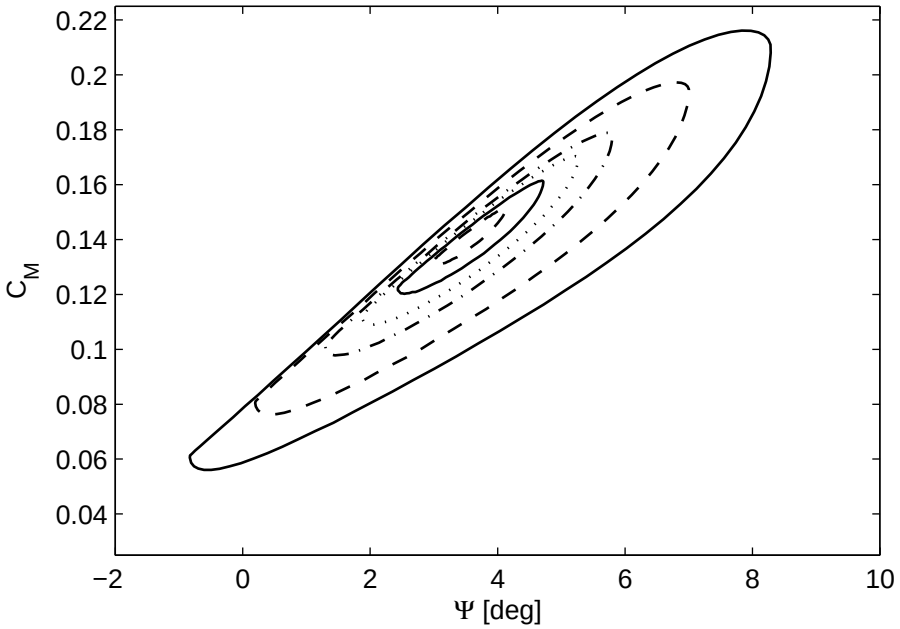

(b) Loops with the rheologic element

Figure 20: Effect of the rheologic element on the numerical simulation of the hysteresis loops of Fig.12

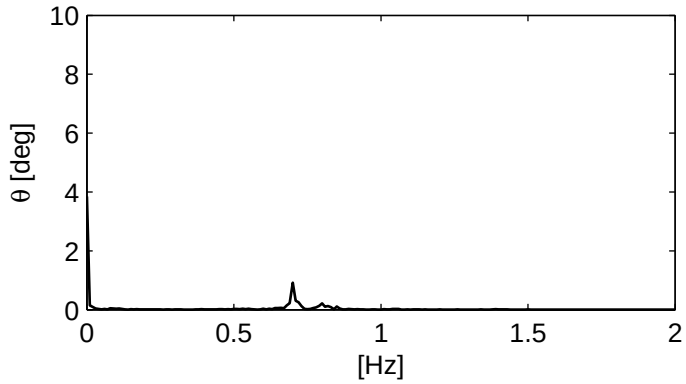

(a) $\frac{w}{V} = 0.5°$ at $0.7\ Hz$

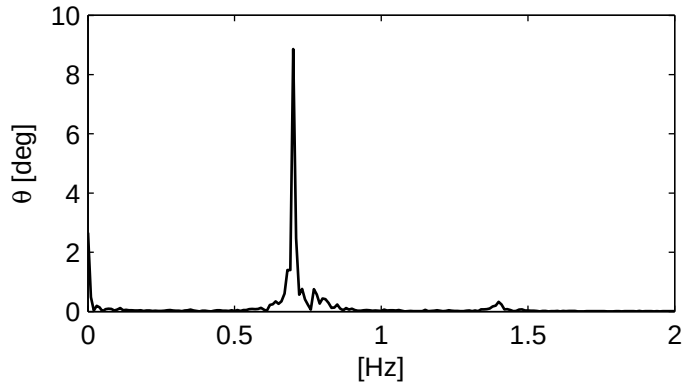

(b) $\frac{w}{V} = 1°$ at $0.7\ Hz$

Figure 21: Numerical frequency response of the aeroelastic model under two different turbulent wind conditions

6 Concluding remarks

The aerodynamic instability was studied on a deck section model by specific tests performed in wind tunnel and by numerical simulations. The instability driven by the stall of the moment coefficient may be reached because of large variations of the instantaneous angle of attack due to the combination of deck motion and turbulent wind components. The comparison of analyses with both a linear and a nonlinear approaches highlights the necessity of considering the nonlinear effects of large variations of the instantaneous angle of attack, during both experimental tests and numerical simulations. The representation of aerodynamic forces by means of hysteresis cycles appears to be an effective tool for taking into account aerodynamic nonlinearities.

References

Caracoglia, L., Jones, N. P., 2003. Time domain vs. frequency domain characterization of aeroelastic forces for bridge deck sections. J. Wind Eng. Ind. Aerodyn. 91 (3), 371–402.

Chen, X., Kareem, A., 2001. Nonlinear response analysis of long-span bridges under turbulent winds. J. Wind Eng. Ind. Aerodyn. 89 (14-15), 1335–1350.

Chen, X., Kareem, A., 2003. Aeroelastic analysis of bridges: Effects of turbulence and aerodynamic nonlinearities. Journal of Engineering Mechanics 129 (8), 885–895.

Chen, X., Matsumoto, M., Kareem, A., 2000. Time domain flutter and buffeting response analysis of bridges. Journal of Engineering Mechanics 126 (1), 7–16.

Diana, G., Bruni, S., Rocchi, D., 2005. A numerical and experimental investigation on aerodynamic non linearities in bridge response to turbulent wind. In: Proceedings of the EACWE 4, Prague CR.

Diana, G., Falco, M., Bruni, S., Cigada, A., Larose, G., Damsgaard, A., Collina, A., 1995. Comparisons between wind tunnel tests on a full aeroelastic model of the proposed bridge over stretto di messina and numerical results. J. Wind Eng. Ind. Aerodyn. 54-55, 101 – 113.

Diana, G., Resta, F., Rocchi, D., 2007. A new approach to model the aeroelastic response of bridges in time domain by means of a rheological model. In: Proceedings of the ICWE 12, Cairns Australia.

Diana, G., Resta, F., Rocchi, D., 2008a. A new numerical approach to reproduce bridge aerodynamic non-linearities in time domain. J. Wind Eng. Ind. Aerodyn. 96 (10-11), 1871 – 1884.

Diana, G., Resta, F., Rocchi, D., Argentini, T., 2008b. Aerodynamic hysteresis: wind tunnel tests and numerical implementation of a fully non linear model for the bridge aeroelastic forces. In: Proceedings of the AWAS 08, Jeju, Korea.

Diana, G., Resta, F., Zasso, A., Belloli, M., Rocchi, D., 2004. Forced motion and free motion aeroelastic tests on a new concept dynamometric section model of the messina suspension bridge. J. Wind Eng. Ind. Aerodyn. 92 (6), 441–462.

Hartley, R., Zisserman, A., 2003. Multiple View Geometry in Computer Vision, 2nd Edition. Cambridge University Press, Cambridge.

Jain, A., Jones, N. P., Scanlan, R. H., 1996. Coupled aeroelastic and aerodynamic response analysis of long-span bridges. J. Wind Eng. Ind. Aerodyn. 60 (1-3), 69–80.

Minh, N. N., Miyata, T., Yamada, H., Sanada, Y., 1999. Numerical simulation of wind turbulence and buffeting analysis of long-span bridges. J. Wind Eng. Ind. Aerodyn. 83, 301–315.

Zasso, A., 1996. Flutter derivatives: advantages of a new representation convention. J. Wind Eng. Ind. Aerodyn. 60 (1-3), 35–47.

Zhang, X., Xiang, H., Sun, B., 2002. Nonlinear aerostatic and aerodynamic analysis of long-span suspension bridges considering wind-structure interactions. J. Wind Eng. Ind. Aerodyn. 90 (9), 1065–1080.